Hindawi
Mathematical Problems in Engineering
Volume 2019, Article ID 1629391, 13 pages
https://doi.org/10.1155/2019/1629391

Research Article

Molecular Structure Characteristics and Wetting Behaviors of Alkyl Binary Doped Ionic Liquids' Thin Lubricating Films on Silicon Surfaces: Molecular Dynamics Simulations

Sisi Liu,[1,2] **He Sun**,[1] **Xiaoning Huang**,[1] **Shuangshuang Ruan**,[1] **Haixu Lu**,[1] **Zhicheng Tang**,[1] **and Yunwen Wu**[1]

[1]*School of Mechanical Engineering, Xiangtan University, Xiangtan 411105, China*
[2]*Engineering Research Center of Complex Tracks Processing Technology and Equipment of Ministry of Education, Xiangtan University, Xiangtan 411105, China*

Correspondence should be addressed to Sisi Liu; liusisi@xtu.edu.cn

Received 7 June 2019; Accepted 25 July 2019; Published 20 October 2019

Guest Editor: Qijun Zheng

The molecular structure characteristics and wetting behaviors of alkyl binary doped ionic liquids' (ILs) thin lubricating film on silicon surfaces, which are composed of a (DA) self-assembled monolayer (SAM) and a binary doped ILs layer, are probed by molecular dynamics simulations. In the binary doped ILs layer, 1-carboxyethyl-3-methylimidazolium chloride ([CMIM]Cl) ILs were bonded to the terminal amino (NH_2) groups of the DA SAM, and 1-dodecyl-3-methylimidazolium hexafluorophosphate ([DMIM]PF_6) ILs were distributed around the [CMIM]Cl molecules by physical adsorption. Additionally, surface coverage and chain grafting positions of the bonded-phase [CMIM]Cl and the adsorption properties of mobile-phase [DMIM]PF_6 were investigated. The simulation results revealed that the optimal surface coverage of [CMIM]Cl on the DA SAM was 50% with a lateral spacing of $2a$ and a longitudinal spacing of $2\sqrt{2a}$, in which a is the space between the adjacent molecules. Meanwhile, the optimal molecular ratio of [CMIM]Cl to [DMIM]PF_6 was 1 : 4, leading to the stablest structure of the lubricating film. Wetting behaviors of thin lubricating film on silicon surfaces showed good hydrophobicity, which is helpful for reducing friction and adhesion. It can be anticipated that the alkyl binary doped ILs' thin lubricating film is suitable for antifriction and antiadhesion applications on silicon surfaces.

1. Introduction

Ionic liquids (ILs) are organic molten salt that generally combines bulky asymmetric cations with various anions [1]. A number of simulation studies of ILs have been carried out in recent years for its unique physiochemical property. Favorable properties include negligible vapor pressure, large chemical and thermal stability ranges, and often unusual solvation characteristics as well [2]. These variations in properties are tailored by the careful selection and turning of the constituent ions [3]. These characteristics are in line with the desired performance of idealized lubricants, giving it the potential to become a new lubricant with high performance under harsh conditions such as in the fields of engineering fluids and the aerospace and the computer industries [4, 5]. Another promising application of ILs is that they are used as a kind of lubricant in micro/nanoelectromechanical systems (M/NEMS) [6]. The good lubricating performance in M/NEMS is attributed to the surface interactions and tribochemical processes at the interface [7].

The tribological properties of ILs matter to the development of new lubricating materials [8]. A number of studies of ILs have been carried out in recent years. Most studies of ILs have concentrated on the physical and chemical properties and their synergistic effects [9, 10]. Liu et al. found that ILs lubricants have excellent antiwear and antifriction properties and the tribological properties were far superior to the traditional lubricants. Zhao et al. [11, 12]

studied the tribological properties of ILs films with different terminal groups. The different terminal groups showed different physicochemical properties, which affect the micro/nano-tribological properties of the film. Ye et al. [13] believed the reason that the outstanding tribological properties of ILs are ascribed to the stable and orderly transition state of the combination of positive and negative charges in the friction process. Moreover, the transition state can form a lubricating film of boundary thickness and is difficult to be cut. As mentioned above, with excellent antifriction and adhesion-resistance properties, ILs can be widely used in the component design of lubricating films.

The tribological properties of thin lubricating films have an intimate relationship with the surface wetting behaviors [14, 15]. The thin lubricating films with good hydrophobicity and low adhesion and friction are urgently needed in applications of M/NEMS devices. Researchers demonstrated that the self-assembled monolayers (SAMs) on silicon (Si) surfaces can effectively reduce the surface energy in M/NEMS. Lian et al. [16] prepared a single-layer silane SAM on the surface of a titanium alloy by using perfluorooctyltrichlorosilane (FOTS). The results indicated that the titanium alloy surface modified by FOTS showed a good hydrophobic property, while in terms of tribological properties, the FOTS modified surface did not exhibit a good performance. Pu et al. [17] studied the surface-capped ILs as a lubricating phase that possesses good antiwear and antifriction properties. However, the high surface energy leads to a high adhesion, which limits the applications in M/NEMS. For this reason, the synergistic effect of SAMs and ILs could be combined to improve both the hydrophobicity and the antifriction of thin lubricating films.

Imidazolium cation represents by far the most investigated class of ionic ILs. Liu et al. [18] found that PF_6^- exhibited the best antifriction and antiwear properties in the same imidazolium cation at room temperature. Qu et al. [19] researched that the cations with longer side chain showed better antiwear protection for titanium. At room temperature, the best performance was obtained for 8, 9, 1-methyl-3-benzylimidazolium chloride ([BMIM]Cl). Based on the conclusions above, the imidazolium-based ILs [CMIM]Cl and [DMIM]PF_6 are used to compose the alkyl binary doped ILs in our study.

Molecular dynamics (MD) has been widely applied to predict many properties of SAMs [20] and ILs [21]. This approach has been successfully applied for finding the surface binding energy and adsorption behavior between polymers and substrates [22, 23], the interaction between polymers and crystal structures [24], and the interaction between polymers and polymer-metal oxides [25]. Chaumont et al. [26, 27] had used MD simulations to study the behavior of the ILs-water interface and the transport of large solvent molecules across the interface. Maolin et al. [28, 29] investigated the microscopic structures of the imidazolium-based IL 1-butyl-3-methylimidazolium hexafluorophosphate ([BMIM]PF_6) on a hydrophobic graphite surface by MD simulations and showed that both the mass and electron densities of the surface-adsorbed ILs are oscillatory. In addition, some studies have been performed regarding the wetting of graphene with ILs nanodroplets. It has been observed that the contact angle of the nanodroplet increased with its size [30].

However, little information has been obtained on the synthesis effect of the coexistent stationary and mobile phases on the wetting behaviors and friction properties of ILs' thin lubricating films. Moreover, previous research has failed to consider studying the molecular structural characteristics and dynamical nanowetting behavior of the alkyl binary doped ILs' thin lubricating films. In this work, N-[3-(trimethoxysilyl)propyl] ethylenediamine (DA) with one siloxy group was used to modify a Si surface, which was the basic structural material in N/MEMS. The [CMIM]Cl and [DMIM]PF_6 were used to modify the DA SAM, which typically resulted in the formation of the alkyl binary doped ILs' thin lubricating films. As the stationary phase, the [CMIM]Cl molecules chemically reacted with the terminal amino groups of the DA SAM and formed a backbone structure to enhance the load-carrying capacity. In contrast, as the mobile phase, the [DMIM]PF_6 molecules were physically adsorbed on the [CMIM]Cl/DA surface with a low shear rate to reduce the friction coefficient. The results of the good wettability of the films will provide a theoretical basis for its application in the antiadhesion and antiwear fields.

2. Models and Simulation Details

2.1. Models. Apart from the coulombic forces, dispersive forces, and inductive forces, the cation-anion interactions, such as hydrogen-bonding-type interactions play considerable roles in ILs [31, 32]. The optimized molecular structures of the DA, [CMIM]Cl, [DMIM]PF_6, and Si in the simulations are shown in Figures 1(a)–1(d), respectively.

In addition, Figure 1 shows the partial atomic charges of the cations and anions for hydrogen interactions in the system. The strongest hydrogen-bond interaction is attached to the C^2 position of the imidazolium ring cations [33]. The distances of the mass center of Cl^- and PF_6^- from hydrogen are 1.997 Å and 2.853 Å, respectively [34].

In this work, the thin lubricating films were formed on the Si surface by a two-step process. Firstly, DA molecules were bonded to a hydroxyl-terminated Si surface to form a densely packed SAM. The DA SAM with the polar amino group exposed outside was served as a connection layer. Then, the [CMIM]Cl molecules were grafted onto the amino group of DA SAM through an amidation, and the [DMIM]PF_6 molecules were physically absorbed on the [CMIM]Cl layer; thus, the binary doped ILs overlayer was formed on the DA SAM. For convenience, the films derived from DA with [CMIM]Cl or [DMIM]PF_6 are coded as [CMIM]Cl/DA/Si or [DMIM]PF_6/DA/Si, respectively, and the films derived from DA with [CMIM]Cl and [DMIM]PF_6 are coded as [CMIM]Cl&[DMIM]PF_6/DA/Si. With one more $-CH_2CH_2NH-$ unit, DA tends to form a more densely packed and more ordered SAM. Additionally, hydrogen bonding between adjacent molecules may occur in the buried–NH–layer, which will enhance the rigidity and stability of the aminosilane SAM [35]. The schematic representation of the reaction process and

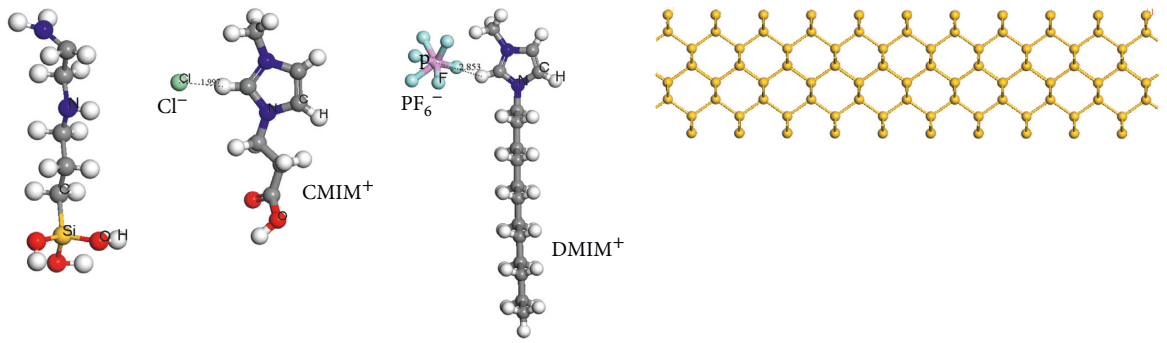

Figure 1: Molecular structures in the simulation system: (a) DA; (b) cation ($CMIM^+$); anion (Cl^-); (c) cation ($DMIM^+$); anion (PF_6^-); and (d) Si substrate.

the ideal structure of the alkyl binary doped ILs thin lubricating film on Si substrate are shown in Figure 2.

The structural organization of the molecules assembling on a surface is strongly affected by the various energy contributions within the system. Earlier theoretical and experimental studies have already suggested that molecular structures such as the surface coverage and the chain grafting positions can affect the chemical reactivity of the functional groups on the surfaces, which further impact the wetting behavior of the thin lubricating film. The surface coverage and the chain grafting positions of DA molecules on Si substrates have already been proved in our previous work by MD simulations [36]. Hence, the surface coverage and the chain grafting positions of [CMIM]Cl molecules grafted on DA surface have also been examined in this paper.

The simulation models that comprise the thin lubricating film applied in the system were constructed successively. Firstly, to simulate the surface coverage of [CMIM]Cl on the DA SAM, a slab of a Si crystal without a hydroxylated surface was cleaved at the Si (100) plane and a 4 nm vacuum layer was added to it, which is used as the Si base unit. According to our previous study, when the surface coverage of the DA molecules on the Si substrate was 50%, the corresponding energy per chain was the lowest and the structure of the final monolayer was the stablest [37]. In addition, the substitution patterns of the 1×4 and 1×5 cells were selected, in which 1 represents the number of rows and 4 or 5 represents the number of lines. The patterns are shown in Figure 3. Clearly, a [CMIM]Cl molecule grafted onto the DA SAM surface in an arbitrary position was used to derive the [CMIM]Cl molecular surface coverage simulation models. Specially, the ratio of the number of grafted [CMIM]Cl molecules to DA molecules was considered as the surface coverage rate of the [CMIM]Cl molecules.

On account of the $[DMIM]PF_6$ molecules physically adsorbed rather than grafted on the surface of [CMIM]Cl/DA/Si, the simulated model of adsorption was different from the surface cover age simulation model. The [CMIM]Cl/DA/Si layer and the amorphous structural $[DMIM]PF_6$ layers with different ratios were constructed. In addition, two independent layers were grouped together to obtain the simulated model, as shown in Figure 4.

Wetting behaviors of the nanoscale water droplets on the OH/Si, DA/Si, $[DMIM]PF_6$/DA/Si, and [CMIM]Cl& $[DMIM]PF_6$/DA/Si surfaces were studied, which could reflect the antiadhesion properties of all the films. Specifically, constructions of the wetting simulated models were based on the optimal surface coverage and chain grafting positions. The DA SAM unit was extended into a $20 \times 20 \times 2$ super cell to obtain a surface with the size of $76.8 \times 76.8 \times 89.5$ Å^3. A water nanocluster containing 483 water molecules was placed onto the surfaces of 4 kinds of samples. The dimension along the z-axis was set to 89.5 Å so that the water can be large enough to exhibit the bulk behavior. The wetting behaviors simulation models are depicted in Figure 5.

2.2. Simulation Details. Molecular dynamic simulations were carried out with the Discover and Amorphous Cell module in Materials Studio of Accelrys Inc. The models of the Si substrate, a DA connection-layer, a bonded-phased [CMIM]Cl, a mobile-phased $[DMIM]PF_6$, and a nano-water droplet were constructed. Firstly, the Si lattice was derived from the structural database of Materials Studio and cleaved along the (100) and extended into a super cell. The lattice space group is Fd3m and the lattice concrete parameters are $a = b = c = 0.543$ and $\alpha = \beta = \gamma = 90^\circ$. Secondly, the surface was completely hydroxylated. The DA molecules were bonded to the hydroxylated Si substrate, the [CMIM]Cl molecules were grafted on the external surface of DA SAM, and the $[DMIM]PF_6$ molecules were dissociated on the [CMIM]Cl surface. Finally, a nano-water droplet was placed on the outside surface of the $[DMIM]PF_6$ molecular layer.

The COMPASS [38] (condensed-phase-optimized molecular potentials for the atomistic simulation studies) force field, which is based on the *ab initio* and empirical parameterization techniques, was used in the whole simulation for its ability to predict the total structural parameters for some ILs with available parameters [39]. The total potential energy is expressed as

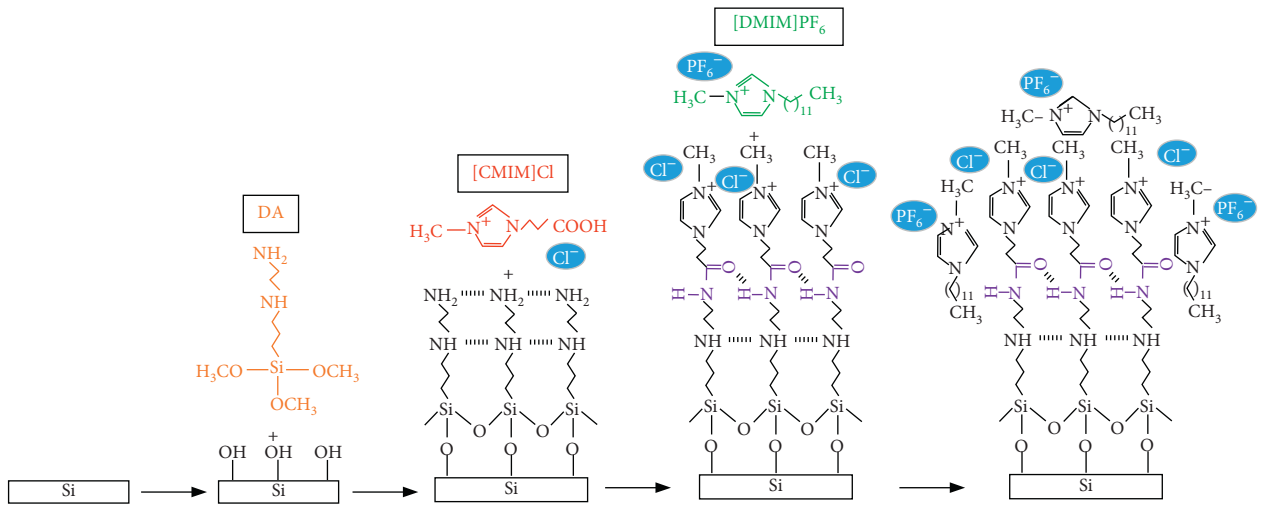

Figure 2: Schematic representation of the reaction process of the alkyl binary doped ILs' thin lubricating film on Si surface. The color code is as follows: DA molecules (orange); cations of [CMIM]Cl (red); amide bonds (purple); cations of $[DMIM]PF_6$ (green); and anions (blue).

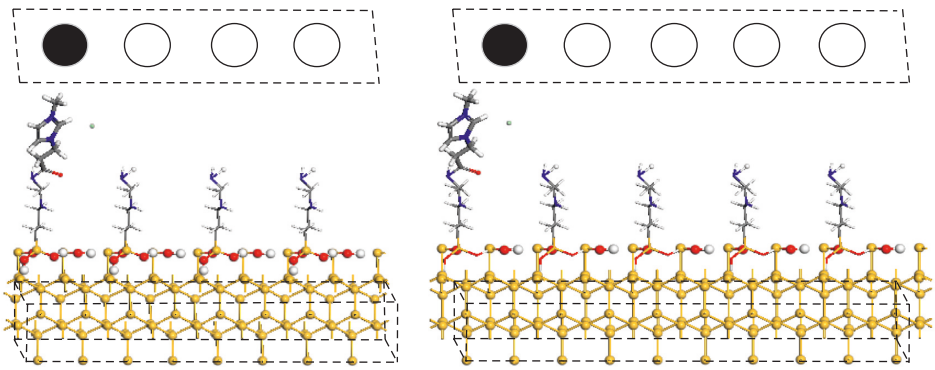

Figure 3: Molecular modeling of the [CMIM]Cl molecular coverage simulation system: (a) 1×4 cells; (b) 1×5 cells. The color code is as follows: oxygen atoms (red); hydrogen atoms (white); nitrogen atoms (blue); carbon atoms (gray); and Si atoms (yellow).

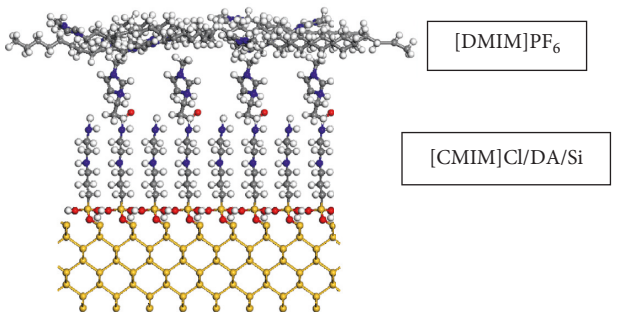

Figure 4: Molecular simulation modeling of the adsorption. The color code is as follows: oxygen atoms (red); hydrogen atoms (white); nitrogen atoms (blue); carbon atoms (gray); and Si atoms (yellow).

$$
\begin{aligned}
E_{\text{total}} &= E_{\text{b}} + E_{\theta} + E_{\phi} + E_{\chi} + E_{\text{cross}} + E_{\text{nonbond}} \\
&= \sum_{b} \left[k_2 (b - b_0)^2 + k_3 (b - b_0)^3 + k_4 (b - b_0)^4 \right] \\
&\quad + \sum_{\theta} \left[k_2 (\theta - \theta_0)^2 + k_3 (\theta - \theta_0)^3 + k_4 (\theta - \theta_0)^4 \right] \\
&\quad + \sum_{\phi} \left[k_1 (1 - \cos \phi) + k_2 (1 - \cos 2\phi) + k_3 (1 - \cos 3\phi) \right] \\
&\quad + \sum_{\chi} k_2 (\chi - \chi_0)^2 + \sum_{ij} \varepsilon_{ij} \left[2 \left(\frac{r_{ij}^0}{r_{ij}} \right)^9 - 3 \left(\frac{r_{ij}^0}{r_{ij}} \right)^6 \right].
\end{aligned} \tag{1}
$$

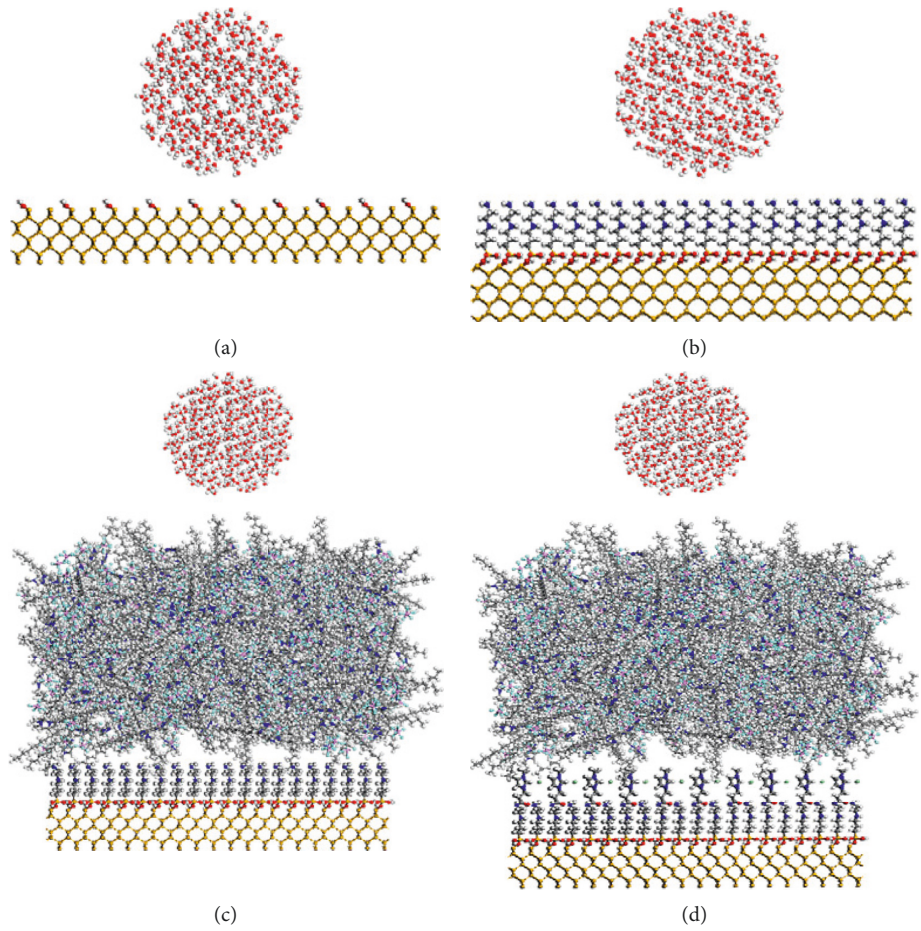

Figure 5: Snapshots of the wetting behaviors simulation models at the beginning of the simulation: (a) OH/Si; (b) DA/Si; (c) [DMIM]PF_6/DA/Si; and (d) [CMIM]Cl&[DMIM]PF_6/DA/Si. The color code is as follows: oxygen atoms (red); hydrogen atoms (white); nitrogen atoms (blue); carbon atoms (gray); and Si atoms (yellow).

The potential functions can be divided into two parts: the diagonal and off-diagonal cross-coupling terms and the nonbonded interaction terms. The diagonal and off-diagonal cross coupling terms include E_b, E_θ, E_ϕ, and E_χ for bond, angle, torsion, and out-of-plane angle coordinates, respectively, and the E_{cross} for the cross-coupling terms between internal coordinates. The cross-coupling terms are important for predicting vibrational frequencies and structural variations associated with conformational changes. The nonbonded terms, which include a Lennard-Jones 9-6 (L-J) potential for the VDW interactions and a Coulombic term for the electrostatic interactions, are used for interactions between pairs of atoms that are separated by three or more intervening atoms, or those that belong to different molecules. The detailed parameters of [CMIM]Cl and [DMIM]PF_6 are reported in Tables 1 and 2 of Supplementary Materials.

The solid Si substrate was frozen during all simulations to enhance the computational efficiency. The canonical ensemble NVT (absolute temperate-T, constant number of particles-N, and constant volume-V) was performed at 298 K for each system using the velocity-Verlet algorithm. The integration step was set as 1 fs. The temperature was controlled by using a Nosé–Hoover thermostat with a damping parameter 1.0 ps^{-1}. When using the atom-based summation method to calculate van der Waals (VDW) force and the group-based calculation method to calculate the coulombic force, the cutoff radius was 12.5 Å. To eliminate the effects of the edges, periodic boundary conditions were considered for both x and y directions, while nonperiodic and mirror boundary conditions were applied along the z-axis. Initially, the Smart minimizer in the discovery module performed 20,000 iterations for the energy calculation and structural optimization until equilibrium to obtain the minimum energy system. Moreover, in the wetting behavior simulations, the models were allowed to equilibrate by a sequence of 1000 ps dynamics simulations at a constant pressure of 1 atm to ensure that the models are equilibrize well.

3. Results and Discussion

3.1. Surface Coverage of the [CMIM]Cl Molecules on the DA SAM Surface. Molecules with a lower energy per chain and less twist deformation are more stable with little intermolecular interactions. According to our previous work,

when the surface coverage of the DA molecules on the Si substrate was 50%, the corresponding energy per chain was the lowest, and the structure of the DA SAM was the stablest. In this work, the energy per chain is used to estimate the stability of the [CMIM]Cl/DA dual-layer film. The energy per chain of the [CMIM]Cl molecules in the simulation system is calculated by the following equation:

$$E_{\text{ave}} = \frac{E - E_0}{n}, \tag{2}$$

where E is the total energy, which is the mean value of the energy with various grafting positions at the same surface coverage, E_0 is the energy when the surface coverage is zero, and n indicates the number of [CMIM]Cl molecules at the corresponding surface coverage.

The relationship between the energy per chain and the surface coverage of the [CMIM]Cl molecules on the DA SAM surface is shown in Figure 6. The simulation results show that when the surface coverage is 50%, the energy per chain of the [CMIM]Cl molecules is the lowest, which indicates that the structure of the [CMIM]Cl/DA dual-layer film is the stablest at this time. Therefore, the optimal surface coverage of the [CMIM]Cl molecules on the DA SAM surface is 50%, which is in good agreement with the experimental results, and the possible reason is that the packing of alkyl chains and aromatic groups plays a primary role in determining the substitution further influencing the surface coverage.

3.2. Chain Grafting Position Analysis of [CMIM]Cl Molecules on DA SAM Surface. The distance between molecules is an important factor affecting the system energy. In the $4 \times 4 \times 1$ cell simulation system with 50% surface coverage of [CMIM]Cl molecules on the DA surface, there are several grafting positions of the [CMIM]Cl molecules. Setting the distances of adjacent two Si atoms as a, the feasible grafting positions are shown in Figure 7(a), and the possible distances between two arbitrary [CMIM]Cl molecules are $\sqrt{2a}$, $2a$, $2\sqrt{2a}$, $\sqrt{10a}$, and $3\sqrt{2a}$. According to the combined calculation method, there are 9, 8, 4, 4, and 1 arrangements at the same distances. The mean energy per chain of the [CMIM]Cl molecules with different spacings is simulated, and the results are shown in Table 1; the error is the difference between the energy per chain and the average energy per chain with different arrangements and the same distance.

Generally, the energy per chain is calculated to obtain the optimal chain grafting positions. From the data in Table 1, it can be clearly seen that when lateral spacing is $2a$ and the longitudinal spacing is $2\sqrt{2a}$, the energy per chain is the lowest due to the smallest intermolecular interactions. However, no matter how the distance changes, the energy per chain gradually increases because of the strongest repulsive interactions between molecules at close distances and the emergence of single molecule lodging or torsion deformation at large distances. Moreover, both the strong repulsive interaction and lodging or torsion deformation lead to the instability of the overall molecular film. The above analyses demonstrate that the position of adjacent two IL

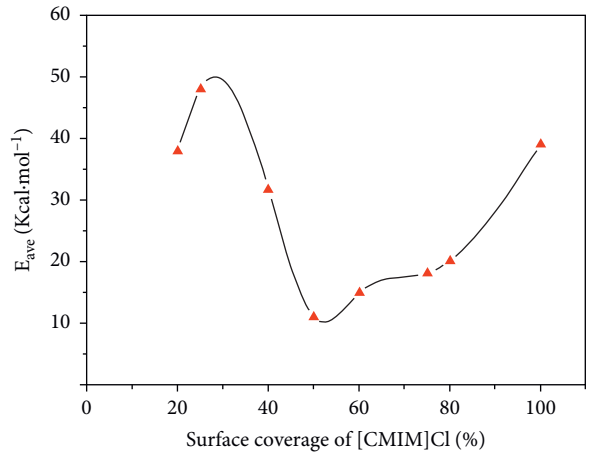

Figure 6: Energy per chain of the [CMIM]Cl/DA dual-layer film with different [CMIM]Cl molecular surface coverages.

molecules require a certain range. It is further concluded that when the [CMIM]Cl molecular surface coverage is 50% with a longitudinal spacing of $2\sqrt{2a}$ and a lateral spacing of $2a$ arrangement, the molecular sequence is relatively dense and orderly, and the optimal chain grafting positions are shown in Figure 7(b). The position is similar to a zigzag distribution. It is because the van der Waals interactions between chains are favorable. As the chains are at suitable distances, they have increasing rotational freedom to reorient themselves to low-energy configurations. There is ample room for the chains to move away from the surface. It is reported that the relative density and relative orderliness of the arrangement can effectively enhance the stability of the system [40].

3.3. Simulation Analysis of [DMIM]PF_6 Molecular Adsorption Model. The model of an $8 \times 8 \times 2$ Si unit cell with 50% grafted DA molecules and 50% [CMIM]Cl molecules grafted on the DA surface as the substrate, namely, [CMIM]Cl/DA/Si as mentioned above, and the amorphous structural [DMIM]PF_6 as the adsorbed layers were utilized. The [DMIM]PF_6 layers were chosen based on the ratio of the number of [CMIM]Cl and [DMIM]PF_6 molecules, which were from 1 : 1 to 1 : 10, respectively. After the dynamics simulation, it was found that there was no significant difference in the equilibrium adsorption structures of the [DMIM]PF_6 layer on the surface of the [CMIM]Cl/DA/Si. To further analyze the interaction between the adsorption layer and the adsorbed layers, the adsorption energy of the [DMIM]PF_6 layers on [CMIM]Cl/DA/Si was quantitatively calculated. The binding energy of the interface can be used to measure the bonding strength of the interface. The greater the interface binding energy is, the more work it takes to destroy the interface with an interface that is more solid. The binding energy, E_{binding}, is the negative value of interaction energy of the $E_{\text{adsorption}}$. A higher value of the binding energy implies stronger interactions or attachments. And the equations are as follows:

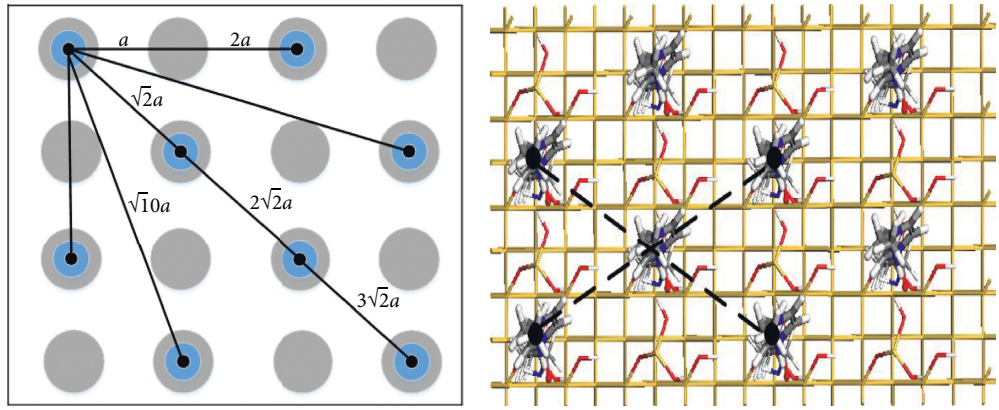

(a) (b)

Figure 7: (a) The possible distances between two [CMIM]Cl molecules in the $4 \times 4 \times 1$ cell simulated system; (b) the optimal chain grafting positions of the [CMIM]Cl molecules at 50% surface coverage. The color code is as follows: the black indicates the [CMIM]Cl molecule's positions; the blue indicates the DA molecule's positions; and the gray indicates the Si substrate.

Table 1: Average energy per chain of [CMIM]Cl molecule with different spacings.

Orientations	Spacings	Average energy per chain (Kcal/mol)
Lateral spacing	$2a$	−60.178 (±0.13)
Longitudinal spacings	$\sqrt{2a}$	−57.383 (±0.08)
	$2\sqrt{2a}$	−61.417 (±0.10)
	$\sqrt{10a}$	−57.997 (±0.12)
	$3\sqrt{2a}$	−57.708 (±0.15)

$$E_{\text{adsorption}} = E_{\text{total}} - E_{\text{molecule}} - E_{\text{surface}},$$
$$E_{\text{binding}} = -E_{\text{adsorption}}, \quad (3)$$

where $E_{\text{adsorption}}$ is the interfacial adsorption energy; E_{total} is the total energy of the [DMIM]PF_6 layer and the [CMIM]Cl/DA/Si layer; $E_{\text{molecules}}$ is the single point energy of the [DMIM]PF_6 layer; E_{surface} is the single point energy of the [CMIM]Cl/DA/Si layer; and E_{binding} is the interfacial binding energy.

The adsorption energy per chain of the [DMIM]PF_6 molecules was calculated to produce more accurate simulated results. The per chain adsorption energy of the [DMIM]PF_6 molecule at different ratios is shown in Figure 8. When the ratio reaches to 1 : 4, the per chain adsorption energy is the lowest because the intermolecular interactions of a single molecule decreased for a suitable number of [DMIM]PF_6 molecules. In contrast, the binding energy is the highest at a ratio of 1 : 4, which indicates the stablest structure. Obviously, it is concluded that when the molecular number ratio of [CMIM]Cl : [DMIM]PF_6 is 1 : 4, the binding energy between the [DMIM]PF_6 layer and the [CMIM]Cl/DA/Si layer is the largest, and the interface at this time demonstrates the most solid combination.

3.4. Simulation Analysis of the Energy for the Adsorption Model Systems. The [DMIM]PF_6 layers in the mixed amorphous structure are able to bind to the [CMIM]Cl/DA/Si layer because of the existence of intermolecular interactions, i.e., mainly van der Waals and electrostatic forces, of which the VDW forces include both repulsive and dispersive forces. The energy compositions of the molecular system at different ratios are shown in Table 2. It is observed that the VDW repulsive force and the dispersion force in the nonbonding terms contribute the most to the energy of the system. In the bonding term, the bond angle bending energy and the torsion energy are also large, both of which come from the interaction between atoms in the [DMIM]PF_6. However, these energies have no effect on the whole interfacial binding because the energy values are offset from the bonding term in the single point energy of the [DMIM]PF_6 molecules when calculating the binding energy of the interface. It is concluded that the main factor affecting the interface binding is the VDW forces among the interfacial structure molecules.

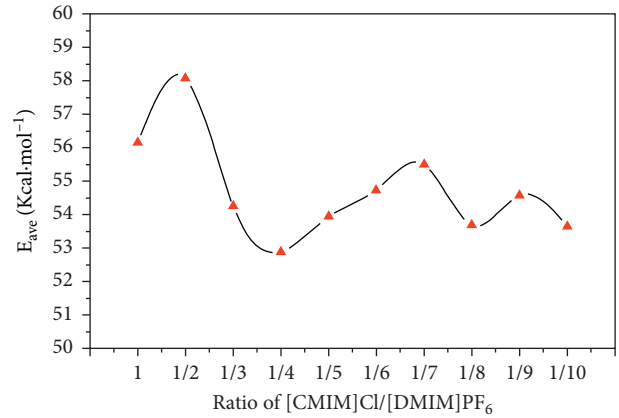

Figure 8: Adsorption energy per chain of the [DMIM]PF_6 molecules at different ratios.

3.5. Wetting Behaviors of the Binary Doped ILs' Thin Lubricating Films. The solid surface wetting property is one of the important properties of materials, which is determined by

Table 2: Energy compositions of the molecular system at different ratios.

Ratios ([CMIM]Cl : [DMIM]PF_6)	Internal energy (kJ/mol)				Nonbond energy (kJ/mol)			
	Bond	Angle	Torsion	Out-of-plane	Cross terms	VDW repulsive	VDW dispersive	Electrostatic
1 : 1	190.7	1206.3	−2061.6	2.4	−172.9	5021.5	−6716.5	−1657.2
1 : 2	224.2	1355	−2480	2.3	−242.5	5652.3	−7529.1	−1738.1
1 : 3	256.9	1508.5	−2885.7	2.4	−299.9	6296.6	−8396.9	−1814.3
1 : 4	291.8	1676.9	−3296.1	3.8	−381.7	6762.6	−9011.5	−1930.5
1 : 5	325.5	1836.1	−3701.8	4.5	−442.2	7390.1	−9831.6	−2078.2
1 : 6	361.8	1979.9	−4120.5	4.8	−517.6	7998.9	−10645.8	−2145.3
1 : 7	398.5	2151.9	−4543.9	5.5	−578.4	8466.5	−11238.7	−2221.2
1 : 8	492.5	2505.3	−4850	5.9	−662.7	8995.7	−11699.1	−4051.9
1 : 9	519.0	2645.5	−5292.8	7.4	−738.9	9478.5	−12327.3	−4193.9
1 : 10	502.7	2632.6	−5769.7	7.1	−791.7	10436.1	−13824.1	−2547.5

the chemical composition of the surface and the microstructure, and it is usually characterized by the contact angle of the liquid on the solid surface [41]. The models, OH/Si, DA/Si, [DMIM]PF_6/DA/Si, and [CMIM]Cl&[DMIM]PF_6/DA/Si lubricating films with the optimal parameters above, and nano-water droplets placed onto the film surfaces to form the wetting systems, were examined by dynamical simulations. Snapshots from the simulations of 4 kinds of surfaces are summarized in Figure 9, which provide an intuitive visual of the wetting character of all the thin lubricating films with different terminal groups (-OH, -NH_2, and -CH_3) from most hydrophobic to the most hydrophilic. In Figure 9, each row of the snapshots corresponds to one kind of film, which is noted along the y-axis. From left to right, 4 conformation snapshots are presented for the simulation steps. At first, the nano-water droplets are ball-shaped on all surfaces. As the simulation proceeds, the ball-shaped configuration of the nano-water droplets are spreading owing to the strong interactions between nano-water droplets and the hydrophilic surfaces (OH/Si and DA/Si), by the reason of the high surface energy functional groups outside the films. The nano-water droplets spread rapidly onto the surfaces possessing an arc-shaped configuration. In contrast, the interactions between nano-water droplets and the hydrophobic surfaces ([DMIM]PF_6/DA/Si and [CMIM]Cl&DMIM]PF_6/DA/Si) are weak, and the equilibrium configuration of nano-water droplets is changed little. The microscopic reason of the phenomenon is the water molecules can form O-H...O and N-H...N hydrogen-bonds on the hydrophilic surfaces of OH/Si and DA/Si, which carry the terminal groups of -OH and -NH_2. So the nano-water droplets spread over the hydrophilic surface gradually with the simulated time increase. The nano-water droplets on the -CH_3 terminated films maintain a ball shape during the simulation without forming a hydrogen bond. Minimal interaction between water molecules and the film surface means that the nano-water droplets cannot spread over the hydrophobic surface. Furthermore, the [CMIM]Cl&DMIM]PF_6/DA/Si shows the optimal hydrophobic phenomenon because of the existence of halogen atoms in [CMIM]Cl, which can form a halogen bond with the cations. In addition, the synergistic effect of hydrogen-bonded and halogen-bonded species facilitates reduced interactions between the ILs, which regulate better hydrophobic properties [42]. When the interfacial binding energy between [DMIM]PF_6 and [CMIM]Cl is negative, the repulsive force of [CMIM]Cl and [DMIM]PF_6 increases, which makes the [DMIM]PF_6 layer more detached, and further increases the antifriction and antiwear properties of the thin lubricating film. The bonded-phase [CMIM]Cl improves the visbreaking and load-bearing properties of the films. It is of great significance to provide theoretical guidance in the field of antifriction and antiadhesion in high-performance thin lubricating films.

To quantitatively describe the wettability of the surface, the contact angles of nano-water droplets on each surface were calculated, which directly reflect the surface hydrophobicity. In addition, contact angles were calculated by the following equations:

$$\cos\theta = \frac{1-h}{R},$$
$$(R-r)^2 + r^2 = R^2. \tag{4}$$

According to the method proposed by Fan and Cağin [43], nano-water droplets in an equilibrium state are approximated as part of an ideal sphere, as shown in Figure 10. In this figure, h is the height of the nano-water droplets; r is the radius of the nano-water droplets contacting the surface; and R is the radius of the nano-water droplets.

However, due to the anisotropic properties of imidazolium-based ILs caused by the asymmetrical distribution of complex cations and anions, the droplet surface is no longer a regular spherical surface on the nanoscale. Under such circumstances, we estimated the average of 5 consecutive sets of the calculated values within 5 degrees as the final contact angle. The calculated values of the contact angles of nano-water droplets on each surface are shown in Figure 11. Obviously, the alkyl binary doped ILs' thin lubricating film definitely improves the wetting property, which indicates the low adhesion and low friction.

3.6. Equilibrium Criteria of MD Simulation. In the simulation process, the temperature and the energy are used to indicate the equilibrium state of the systems. The

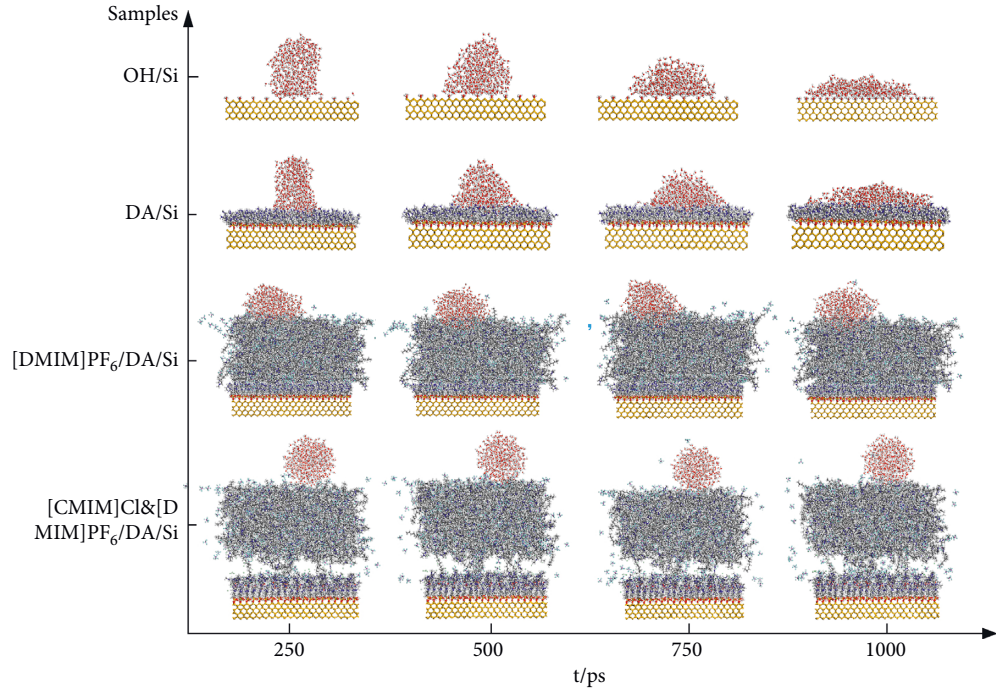

Figure 9: Snapshots of nano-water droplets along the x and y directions at equilibrium state on the surfaces of 4 kinds of ILs' thin lubricating films.

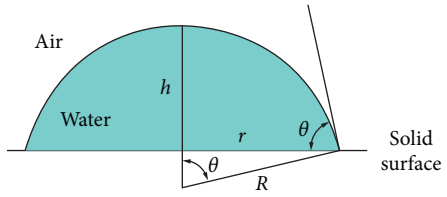

Figure 10: Contact angle calculation diagram.

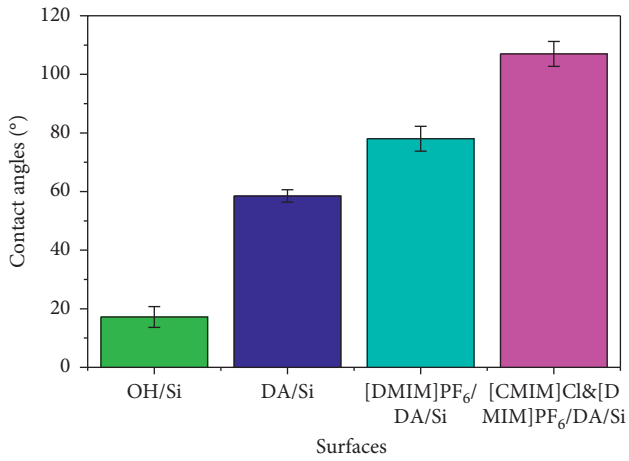

Figure 11: Simulated contact angles of the nano-water droplets on different surfaces.

fluctuations of the temperature and energy in the range of 5–10% are the two protocols of the system equilibrium. In general, the system reaches the equilibrium in the first 50 ps, and an additional 50 ps is allowed in each case to ensure the equilibrium. For example, the temperature and energy fluctuations during the equilibrium operation of the [CMIM]Cl&[DMIM]PF_6/DA/Si system are shown in Figures 12(a)–12(c). It has been observed that the system quickly equilibrates in less than 100 ps and then continues to fluctuate near the equilibrium state. When the equilibrium is reached, the temperature fluctuates within ±20 K, which is 6.7% of the simulated temperature. The deviations of potential energy and nonbond energy are both less than 10%, indicating that the system has reached the energy balance in 1000 ps. Similarly, OH/Si, DA/Si, and [DMIM]PF_6/DA/Si are balanced according to these two protocols, which are widely studied by other researchers [44].

3.7. Radial Distribution Functions. Hydrogen bonds are sufficiently strong to affect the surface wetting behavior [45]. Therefore, to better understand the wetting behaviors of nano-water droplets near different surfaces, the radial distribution function (RDF) is plotted, from which it can be determined whether or not there may be hydrogen bonds. Figure 13 shows the RDF between the water molecules and substrate surface.

Figure 13(a) shows the RDF between the water molecules and the hydroxy in the substrate. The first peak of O-H RDF is located at 1.85 Å, and obviously, (H-O. . .H) hydrogen bonds are formed. Moreover, the hydrogen bonds enhance the hydrophilicity of the OH/Si surface. In the RDF of the DA/Si surface in Figure 13(b), two peaks of N-H are evident at 1.01 to 1.93 Å, which suggest that (N-H. . .N) hydrogen bonds are easily formed and further improve the

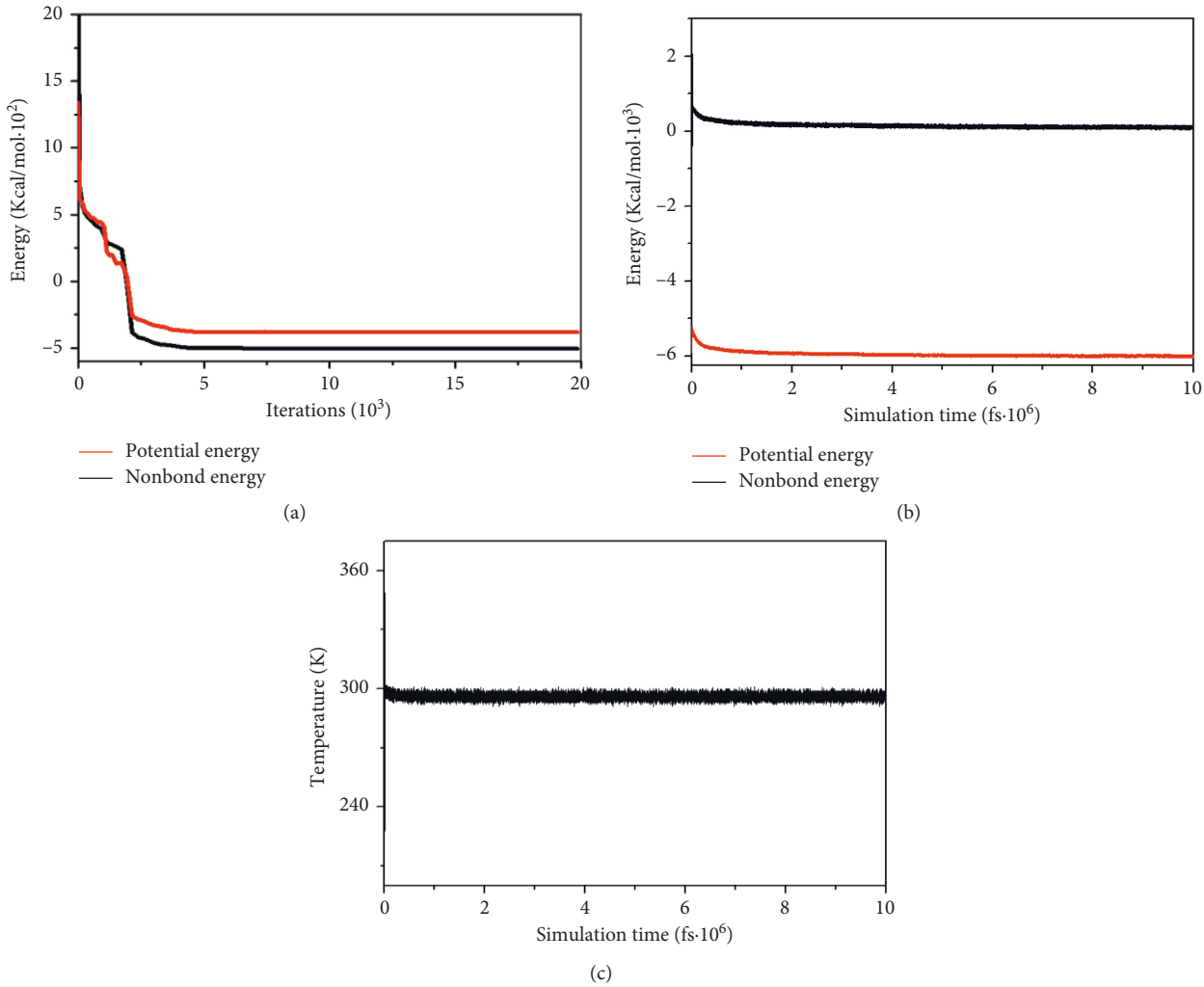

Figure 12: The temperature and the energy fluctuations during the balanced operation of the [CMIM]Cl&[DMIM]PF_6/DA/Si system; (a) energy of the minimum-energy process; (b) energy of the dynamics simulation; and (c) temperature.

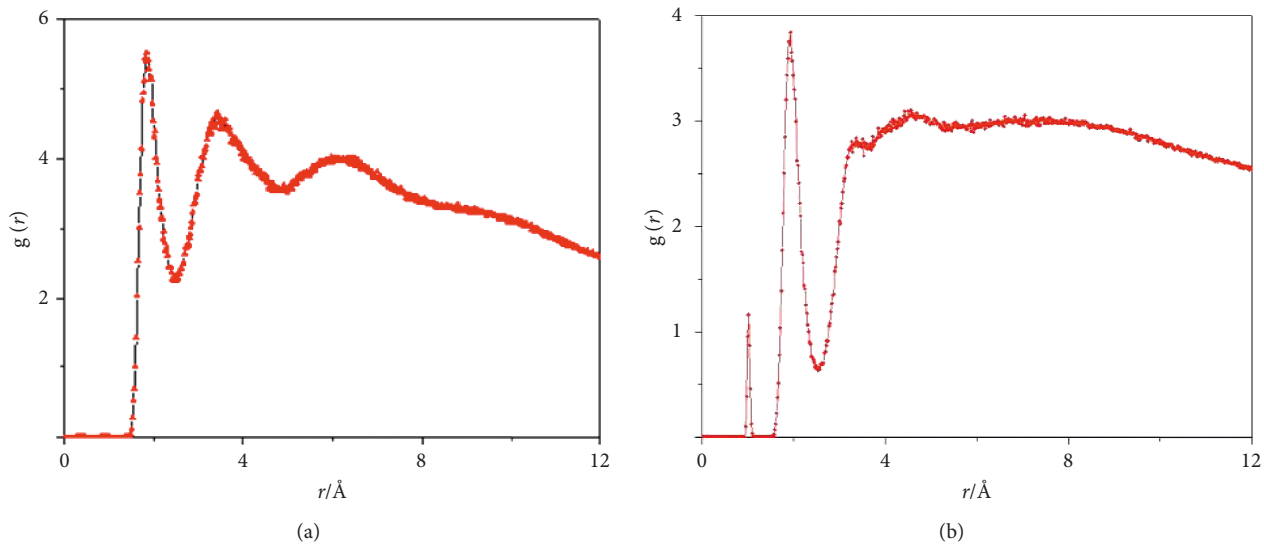

Figure 13: Continued.

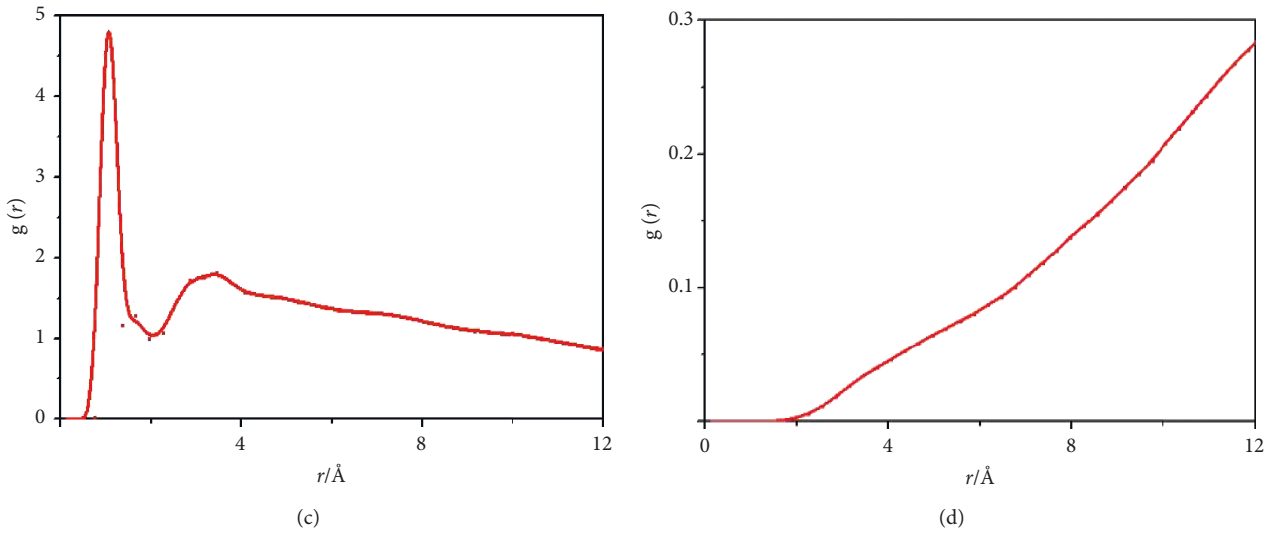

Figure 13: Radial distribution functions between the water molecules and substrate surfaces. (a) OH/Si; (b) DA/Si; (c) [DMIM]PF_6/DA/Si; (d) [CMIM]Cl&[DMIM]PF_6/DA/Si.

hydrophilicity of the DA/Si surface. In Figure 13(c), the RDF between the atoms in water and the atoms in [DMIM]PF_6 demonstrates a peak at 1.05 Å, which suggests that hydrogen bonds are formed with the surface -CH_3 groups, and [DMIM]PF_6/DA/Si shows a better hydrophobic phenomenon. While for the [CMIM]Cl&[DMIM]PF_6/DA/Si surface shown in Figure 13(d), there is no peak value in the (N-H. . .N) hydrogen bond RDF, in contrast with Figure 13(c). The possible reason is that the halogen bonds generated between the anions and cations in [CMIM]Cl reduce the interactions between the [CMIM]Cl and [DMIM]PF_6 molecules. Thus, the weak VDW force acting on the [CMIM]Cl&[DMIM]PF_6/DA/Si surface ensures good hydrophobicity.

4. Conclusions

In summary, the molecular structure and the dynamic wetting behavior of the alkyl binary doped ILs' thin lubricating film were probed by MD simulations. The most important result of the molecular structure is that [CMIM]Cl has an optimal surface coverage of 50% on the DA SAM with a longitudinal spacing of $2\sqrt{2}a$ and a lateral spacing of $2a$, and the simulated system is the stablest under these conditions. Then, the simulated result for the adsorption of [DMIM]PF_6 indicates that when the ratio of [CMIM]Cl : [DMIM]PF_6 is 1 : 4, the interfacial binding energy between the [DMIM]PF_6 molecules and [CMIM]Cl/DA is the largest and has the stablest configuration. With the optimal parameters above, the nanoscale wetting behavior of the thin lubricating film shows the best hydrophobic phenomenon because the thin film of binary doped ILs leads to a dual-dependent phase with the formation of a [CMIM]Cl bonded phase to reduce the adhesion force and a [DMIM]PF_6 mobile phase to reduce the friction force. This research provides a theoretical basis for designing high-performance friction-reduced adhesion-resistant silicon-based materials and offers theoretical guidance for experimental studies.

Data Availability

The data used to support the findings of this study are included within the supplementary information file.

Conflicts of Interest

The authors declare that there are no conflicts of interest regarding the publication of this paper.

Acknowledgments

This work was supported by the National Natural Science Foundation of China (51405413), Natural Science Foundation of Hunan Province (2018JJ4055), Special Projects of Changsha Zhuzhou Xiangtan National Independent Innovation Demonstration Zone (2018XK2302 and 2017XK2107), Scientific Research Fund of Hunan Provincial Education Department (18B074 and 18C0092).

Supplementary Materials

The parameters of the [CMIM]Cl the [DMIM]PF_6 molecules in simulations are listed in Tables 1 and 2. (*Supplementary Materials*)

References

[1] H. György, M. Sega, K. Sofia, C. Schröder, and M. Jorge, "Intrinsic structure of the interface of partially miscible fluids: an application to ionic liquids," *The Journal of Physical Chemistry C*, vol. 119, no. 51, pp. 28448–28461, 2015.

[2] S. Cowie, P. K. Cooper, R. Atkin, and H. Li, "Nanotribology of ionic liquids as lubricant additives for alumina surfaces," *The Journal of Physical Chemistry C*, vol. 121, no. 51, pp. 28348–28353, 2017.

[3] Y. Han, D. Qiao, L. Zhang, and D. Feng, "Study of tribological performance and mechanism of phosphonate ionic liquids for

steel/aluminum contact," *Tribology International*, vol. 84, pp. 71–80, 2015.

[4] N. K. Myshkin, M. I. Petrokovets, and A. V. Kovalev, "Tribology of polymers: adhesion, friction, wear, and mass-transfer," *Tribology International*, vol. 38, no. 11-12, pp. 910–921, 2005.

[5] Y. Mo, W. Zhao, M. Zhu, and M. Bai, "Nano/micro-tribological properties of ultrathin functionalized imidazolium wear-resistant ionic liquid films on single crystal silicon," *Tribology Letters*, vol. 32, no. 3, pp. 143–151, 2008.

[6] J. J. Parajó, M. Villanueva, I. Otero, J. Fernández, and J. Salgado, "Thermal stability of aprotic ionic liquids as potential lubricants. Comparison with synthetic oil bases," *The Journal of Chemical Thermodynamics*, vol. 116, pp. 185–196, 2018.

[7] B. Karimi, M. Tavakolian, M. Akbari, and F. Mansouri, "Ionic liquids in asymmetric synthesis: an overall view from reaction media to supported ionic liquid catalysis," *Chemcatchem*, vol. 10, no. 15, pp. 3713–3205, 2018.

[8] R. Nanda, G. Rai, and A. Kumar, "Interesting viscosity changes in the aqueous urea-ionic liquid system: effect of alkyl chain length attached to the cationic ring of an ionic liquid," *Journal of Solution Chemistry*, vol. 44, no. 3-4, pp. 742–753, 2015.

[9] X. Liu, F. Zhou, Y. Liang, and W. Liu, "Tribological performance of phosphonium based ionic liquids for an aluminum-on-steel system and opinions on lubrication mechanism," *Wear*, vol. 261, no. 10, pp. 1174–1179, 2006.

[10] Z. Mu, F. Zhou, S. Zhang, Y. Liang, and W. Liu, "Effect of the functional groups in ionic liquid molecules on the friction and wear behavior of aluminum alloy in lubricated aluminum-on-steel contact," *Tribology International*, vol. 38, no. 8, pp. 725–731, 2005.

[11] W. Zhao, Y. Wang, L. Wang, M. Bai, and Q. Xue, "Influence of heat treatment on the micro/nano-tribological properties of ultra-thin ionic liquid films on silicon," *Colloids and Surfaces A: Physicochemical and Engineering Aspects*, vol. 361, no. 1–3, pp. 118–125, 2010.

[12] M. Zhu, J. Yan, Y. Mo, and M. Bai, "Effect of the anion on the tribological properties of ionic liquid nano-films on surface-modified silicon wafers," *Tribology Letters*, vol. 29, no. 3, pp. 177–183, 2008.

[13] C. Ye, W. Liu, Q. Gong, and P. Wang, "Tribological performance of room-temperature ionic liquids as lubricant," *Tribology Letters*, vol. 13, pp. 81–85, 2002.

[14] B. Bhushan, M. Palacio, and B. Kinzig, "AFM-based nano-tribological and electrical characterization of ultrathin wear-resistant ionic liquid films," *Journal of Colloid and Interface Science*, vol. 317, no. 1, pp. 275–287, 2008.

[15] W. Zhao, M. Zhu, Y. Mo, and M. Bai, "Effect of anion on micro/nano-tribological properties of ultra-thin imidazolium ionic liquid films on silicon wafer," *Colloids and Surfaces A: Physicochemical and Engineering Aspects*, vol. 332, no. 2-3, pp. 78–83, 2009.

[16] F. Lian, H. C. Zhang, H. L. Zou, and L. Y. Pang, "Preparation of hydrophobic/superhydrophobic surface on silicon wafer by reactive ion etching and self-assembled monolayers," *Chemical Journal of Chinese Universities*, vol. 32, no. 12, pp. 2833–2837, 2011.

[17] J. Pu, L. Wang, Y. Mo, and Q. Xue, "Preparation and characterization of ultrathin dual-layer ionic liquid lubrication film assembled on silica surfaces," *Journal of Colloid and Interface Science*, vol. 354, no. 2, pp. 858–865, 2011.

[18] W. Liu, C. Ye, Q. Gong, H. Wang, and P. Wang, "Tribological performance of room-temperature ionic liquids as lubricant," *Tribology Letters*, vol. 13, no. 2, pp. 81–85, 2002.

[19] J. Qu, P. J. Blau, S. Dai, H. Luo, H. M. Meyer, and J. J. Truhan, "Tribological characteristics of aluminum alloys sliding against steel lubricated by ammonium and imidazolium ionic liquids," *Wear*, vol. 267, no. 5–8, pp. 1226–1231, 2009.

[20] K. G. Pradip and C. G. Sharon, "Molecular dynamics simulation study of self-assembled monolayers of alkanethiol surfactants on spherical gold nanoparticles," *The Journal of Physical Chemistry C*, vol. 111, no. 43, pp. 15857–15862, 2007.

[21] A. S. Paluch, T. C. Lourenço, F. Han, and L. T. Costa, "Understanding the solubility of acetaminophen in 1-n-alkyl-3-methylimidazolium-based ionic liquids using molecular simulation," *The Journal of Physical Chemistry B*, vol. 120, no. 13, pp. 3360–3369, 2016.

[22] Y. Y. Li, L. Z. Liu, H. Shi, L. Weng, and W. W. Cui, "Effect of hydrophilic and hydrophobic SiO_2 particles on performances of PI/Al_2O_3 composite films," *Key Engineering Materials*, vol. 645–646, pp. 26–31, 2015.

[23] Y. Guan, Q. Shao, W. Chen, S. M. Liu, X. P. Zhang, and Y. Q. Deng, "Dynamic three-dimensional nano-wetting behaviour of imidazolium based ionic liquids probed by molecular dynamics simulation," *The Journal of Physical Chemistry C*, vol. 121, no. 42, pp. 23716–23726, 2017.

[24] H. P. Zhang, X. Lu, Y. Leng et al., "Molecular dynamics simulations on the interaction between polymers and hydroxyapatite with and without coupling agents," *Acta Biomaterialia*, vol. 5, no. 4, pp. 1169–1181, 2009.

[25] B. Prathab, V. Subramanian, and T. M. Aminabhavi, "Molecular dynamics simulations to investigate polymer–polymer and polymer–metal oxide interactions," *Polymer*, vol. 48, no. 1, pp. 409–416, 2007.

[26] A. Chaumont, R. Schurhammer, and G. Wipff, "Aqueous interfaces with hydrophobic room-temperature ionic liquids: a molecular dynamics study," *The Journal of Physical Chemistry B*, vol. 109, no. 40, pp. 18964–18973, 2005.

[27] G. Chevrot, R. Schurhammer, and G. Wipff, "Molecular dynamics simulations of the aqueous interface with the [BMI][PF_6] ionic liquid: comparison of different solvent models," *Physical Chemistry Chemical Physics*, vol. 8, no. 36, pp. 4166–4174, 2006.

[28] S. Maolin, Z. Fuchun, W. Guozhong et al., "Ordering layers of [bmim][PF_6] ionic liquid on graphite surfaces: molecular dynamics simulation," *The Journal of Chemical Physics*, vol. 128, no. 13, pp. 134504–134507, 2008.

[29] C. Merlet, M. Salanne, B. Rotenberg, and P. A. Madden, "Imidazolium ionic liquid interfaces with vapor and graphite: interfacial tension and capacitance from coarse-grained molecular simulations," *The Journal of Physical Chemistry C*, vol. 115, no. 33, pp. 16613–16618, 2011.

[30] S. Malali and M. Foroutan, "Study of wetting behavior of $BMIM^+/PF_6^-$ ionic liquid on TiO_2 (110) surface by molecular dynamic simulation," *The Journal of Physical Chemistry C*, vol. 121, no. 21, pp. 11226–11233, 2017.

[31] S. Zahn, F. Uhlig, J. Thar, and B. Kircher, "Intermolecular forces in an ionic liquid ([Mmim][Cl]) versus those in a typical salt (NaCl)," *Angewandte Chemie International Edition*, vol. 47, no. 19, pp. 3639–3641, 2008.

[32] Y. Gao, L. Zhang, Y. Wang, and H. Li, "Probing electron density of H-bonding between cation-anion of imidazolium-based ionic liquids with different anions by vibrational spectroscopy," *The Journal of Physical Chemistry B*, vol. 114, no. 8, pp. 2828–2833, 2010.

[33] S. Shiyong, Z. Jinfang, Q. Mengnan, Y. Shengrong, and Z. Junyan, "Preparation and tribological behaviors of an

amide-containing stratified self-assembled monolayers on silicon surface," *Langmuir*, vol. 24, no. 1, pp. 105–109, 2008.

[34] S. Liu, J. Tong, and Y. Zhang, "Molecular dynamics simulation of structural properties and wetting behavior of silicon based dual composite self-assembled monolayers," *Acta Materiae Compositate Sinica*, vol. 35, pp. 468–475, 2018, in Chinese.

[35] H. Sun, "COMPASS: an ab initio force-field optimized for condensed-phase applications overview with details on alkane and benzene compounds," *The Journal of Physical Chemistry B*, vol. 102, no. 38, pp. 7338–7364, 1998.

[36] H. Sun, P. Ren, and J. R. Fried, "The COMPASS force field: parameterization and validation for phosphazenes," *Computational and Theoretical Polymer Science*, vol. 8, no. 1-2, pp. 229–246, 1998.

[37] D. Bela and D.-K. Agnes, "Molecular modelling simulations to predict density and solubility parameters of ionic liquids," *Molecular Simulation*, vol. 34, no. 10–15, pp. 1167–1175, 2008.

[38] L. Zhang, K. Wesley, and S. Jiang, "Molecular simulation study of alkyl monolayers on Si (111)," *Langmuir*, vol. 17, no. 20, pp. 6275–6281, 2001.

[39] A. B. Sieval, B. V. D. Hout, H. Zuilhof, and E. J. R. Sudholter, "Molecular modeling of alkyl monolayers on the Si (111) surface," *Langmuir*, vol. 16, no. 7, pp. 2987–2990, 2000.

[40] D. K. Paul and K. Karan, "Conductivity and wettability changes of ultrathin nafion films subjected to thermal annealing and liquid water exposure," *The Journal of Physical Chemistry C*, vol. 118, no. 4, pp. 1828–1835, 2017.

[41] C. J. Wu, K. C. Chu, Y. J. Sheng, and H. K. Tsao, "Sliding dynamic behavior of a nanobubble on a surface," *The Journal of Physical Chemistry C*, vol. 121, no. 33, pp. 17932–17940, 2017.

[42] L. Wang, J. Gao, F. Bi, and C. Liu, "Toward the development of the potential with angular distortion for halogen bond: a comparison of potential energy surfaces between halogen bond and hydrogen bond," *The Journal of Physical Chemistry A*, vol. 118, no. 39, pp. 9140–9147, 2014.

[43] C. F. Fan and T. Cağin, "Wetting of crystalline polymer surfaces: a molecular dynamics simulation," *The Journal of Chemical Physics*, vol. 103, no. 20, pp. 9053–9061, 1995.

[44] M. P. Allen and D. J. Tildesley, *Computer Simulation of Liquids*, University Press, Oxford, UK, 1987.

[45] J. Chai, S. Liu, and X. Yang, "Molecular dynamics simulation of wetting on modified amorphous silica surface," *Applied Surface Science*, vol. 255, no. 22, pp. 9078–9084, 2009.